Mean energy required to produce an electron-hole pair in silicon for photons of energies between 50 and 1500 eV

F. Scholze,[a] H. Rabus, and G. Ulm
Physikalisch-Technische Bundesanstalt, Abbestraße 2-12, 10587 Berlin, Germany

(Received 29 January 1997; accepted for publication 26 May 1998)

The photon energy dependence of the mean energy W required to produce an electron-hole pair in silicon for photons with energies between 50 and 1500 eV was determined from the spectral responsivity of selected silicon photodiodes. The spectral responsivity was measured with a relative uncertainty of less than 0.3% using monochromatized synchrotron radiation whose radiant power was measured with a cryogenic electrical substitution radiometer. In order to deduce W from the spectral responsivity of photodiodes with a relative uncertainty of about 1%, a method for the calculation of photon and electron escape losses from silicon photodiodes was developed and the model for the charge carrier recombination losses was improved. In contrast to recent theoretical and experimental results, a constant value $W=(3.66\pm0.03)$ eV was obtained in the photon energy range from 50 to 1500 eV. The present experimental results are confirmed by calculation of the pair creation energy in silicon from data from the literature for the relevant material properties. The difference from previous theoretical work is due to different assumptions about the influence of the band structure of silicon. © *1998 American Institute of Physics.* [S0021-8979(98)01817-9]

I. INTRODUCTION

Silicon detectors are used in many soft x-ray applications such as x-ray astronomy, x-ray microscopy and spectroscopy, lithography, and radiometry. The detection principle is that the absorbed photon energy produces ionization, which can be measured. The term ionization will be used in this article to denote the creation of nonequilibrium free charge carriers in a solid. The internal quantum yield $\eta(h\nu)$ is defined as the number of electron-hole pairs created per photon of energy $h\nu$ absorbed in silicon. We intend to calculate and measure the mean energy $W(h\nu)=h\nu/\eta(h\nu)$ required to produce an electron-hole pair.

$W(h\nu)$ is a material property of silicon which depends on the nature of the particle to be detected and its energy. For energy dispersive detectors, the mean height of the output pulses for incident monochromatic photons is, in absence of any charge losses, proportional to $h\nu/W(h\nu)$. On the other hand, the spectral responsivity s, is defined as the quotient of the detector output, the photo current I, by the monochromatic detector input, the radiant power Φ, as a function of photon energy: $s=I/\Phi$.[1] After correction for all losses, this is equivalent to $s=e/W$, with e the elementary charge. Thus, alternate ways to determine W are the pulse height method, where the pulse height produced by the detector is measured and the photocurrent method, see, e.g., the discussion in Sec. II of Ref. 2.

Values of W for α, β, and γ radiation with energies of about 100 keV to 1 MeV are reported in Refs. 2, 3, and 4. These values are not yet completely consistent, as, e.g., in Sec. VI of Ref. 2, values of $W=(3.62\pm0.02)$ eV for α and $W=(3.68\pm0.02)$ eV for β radiation are recommended in accordance with, e.g., Ref. 4, while in Ref. 3, nearly equal values of $W=(3.6325\pm0.0025)$ eV for α and $W=(3.631\pm0.0025)$ eV for β radiation were reported. In Ref. 3 these differences are explained by charge trapping effects. Note that for photons the photon energy is converted into kinetic energy of electrons by the photoabsorption process. The quantum yield for photons can thus be derived from the quantum yield for electrons.

For photon energies of a few eV Geist and Wang[5] calculated $\eta(h\nu)$. The functional dependence turned out to be nonmonotonous due to the silicon band structure. Geist and Wang used the results of Alig[6,7] for the quantum yield of the electrons. Alig showed that, for a parabolic band structure, the mean energy required to produce an electron-hole pair is equal for electrons and holes, decreasing slowly above a kinetic energy of 10 eV to an asymptotic value of 3.63 eV. Recently, the influence of the symmetry points of a real band structure was pointed out in a study on the solar cell efficiency.[8] The results of Geist and Wang are, however, qualitatively confirmed by experimental data.[9–11] Differences between the data of different authors may be explained by surface-field-induced avalanche effects of the photoexcited carriers.[12]

In the soft x-ray range, theoretical studies by Geist[13] and Fraser *et al.*[14] are available. Fraser *et al.* calculated W for silicon from 50 eV to 8 keV, and predicted a decrease of W with increasing photon energy and discontinuities at the L- and K-absorption edges, similar to recent results for the mean electron-ion pair creation energy in the gas phase of xenon.[15] According to Fraser *et al.*, the discontinuity at the silicon $L_{2,3}$ edge is about 5% and the value of $W=3.63$ eV at a photon energy of 8 keV coincides with the above cited values for α, β, and γ radiation. Geist calculated W in the energy region from 80 to 110 eV (Ref. 13) and obtained, in

[a]Electronic mail: frank.scholze@ptb.de

 © 1998 American Institute of Physics

Downloaded 19 Jun 2003 to 192.135.10.241. Redistribution subject to AIP license or copyright, see http://ojps.aip.org/japo/japcr.jsp

contradiction to Fraser *et al.*, a discontinuity of only 1% at the $L_{2,3}$ edge.

Experimental values for the energy dependence of W in the soft x-ray region, agreeing with the model of Fraser *et al.*, were derived from CCD detectors using the pulse-height method.[16,17] The measurements in Ref. 16, however, covered only the energy range above 350 eV and were normalized to the asymptotic value of W at the high-energy data points. In Ref. 17, only a few emission line energies were used so that no data in the vicinity of the silicon L edge are available. On the other hand, recent measurements by the photocurrent method in the vicinity of the silicon L edge could not exclude any continuous variations but set an upper limit of 0.5% to the discontinuity at the $L_{2,3}$ edge.[18]

In this article we present a calculation of W for photon energies from 50 eV to 2.5 keV. It is based on the results of Alig for impact ionization by energetic electrons and takes into account the atomic relaxation processes which follow inner shell photoexcitation. Our results suggest a constant W for photon energies as low as 50 eV. This is at variance with the previous theoretical studies cited above.

We use the photocurrent method to determine $W(h\nu)$ from the spectral responsivity $s(h\nu)$ of silicon photodiodes. It is determined by comparison of the response of the photodiode to the response of a cryogenic electrical substitution radiometer (CESR) as primary standard for radiant power measurements.[19] Both detectors were stimulated by monochromatized synchrotron radiation with the same radiant power. W is derived from s by the identity $W=(e/s)s_r$, where s_r is a dimensionless factor, which describes the loss processes. This identity was used in previous work to derive, on the assumption that W does not depend on the photon energy, an average value of $W=(3.68\pm0.07)$ eV[20,21] for the photon energy range from 50 eV to 3 keV by using the second method with undispersed synchrotron radiation of BESSY as a primary source standard.[22]

The determination of the dependence of W on photon energy from the spectral responsivity of photodiodes has suffered up to now from a lack of accurate detectors. The use of the CESR to measure the radiant power for the first time allowed $W(h\nu)$ to be accurately determined by this method. A brief presentation of the results has been communicated as a letter.[23]

It was recently claimed that the pulse-height method is the only way to obtain experimental values for W.[24,25] The basic argument was that the photocurrent method would only yield s_r/W with s_r being unknown. Here, we present a calculation of s_r and include a detailed discussion of the uncertainty contributions to the determination of W, arising from uncertainties in the determination of s_r.

The pulse-height method has the advantage that the number of incident photons needs not be determined independently and the measured spectrum can be used to identify events with incomplete energy absorption or charge collection. In the case of soft x-ray photons, however, the finite energy resolution of the detectors at present available sets a lower limit to the photon energy of about 100 to 200 eV. Furthermore, the large relative width of the Gaussian peak masks any line shape artifacts due to incomplete charge collection. A possible shift of the peak position towards lower energies due to incomplete charge collection is therefore practically not detectable by changes of the line shape.[26] The conclusion that incomplete charge collection is not significant[17,24] because the peak has a Gaussian shape is therefore problematic. Moreover, even if incomplete charge collection is accounted for as in Ref. 16, the results critically depend on the model chosen to describe the line shape, as was demonstrated in Ref. 27 for the K-absorption edge. Furthermore, the determination of W from the pulse-height spectra requires calibration of the pulse heights in units of the elementary charge which is at present possible only by normalization to the quantum yield for photons at higher energies which must therefore be separately known.

Using the photocurrent method, W is determined from the integrated detector output, measured either as accumulated charge or as an ionization current, for a known flux of incident photons of known energy. This method has the advantage that the number of incident photons can be increased to achieve an output signal which is sufficiently high to be measured. That offers the possibility to use this method also for very low photon energies, where the (energy-dispersive) detection of single photons is no longer possible. Specially, we are able to access photon energies well below the silicon $L_{2,3}$ edge.

The amount of incomplete charge collection is a function of the depth at which the photons are absorbed and thus a function of the absorption length. The effects of incomplete charge collection therefore would have to be equal for photon energies of, e.g., 90 and 600 eV, so that measurements at such corresponding photon energies would provide a direct test of changes of W above and below the $L_{2,3}$ edge. This has not yet been achieved by pulse-height measurements. The shift of the Al K fluorescence line discussed in Ref. 17 was most probably due to a chemical shift of the fluorescence line itself and not to the predicted change of W (note added in proof in Ref. 17). The other data presently made available by the pulse-height method cover only the energy range down to 350 eV.[16]

It must be noted that both methods must yield the same result for W respectively η. Provided all loss effects are correctly taken into account, both methods yield $\eta=\langle N_i\rangle=(\Sigma_i N_i)/N_0$, the average of the individual numbers of electron-hole pairs, N_i, created by the N_0 detected photons i. In the pulse-height method, N_i and N_0 can be obtained from the measured spectrum, while the photocurrent method directly yields $\Sigma_i N_i$ and N_0 must be determined separately.

II. THE PTB'S SOFT X-RAY DETECTOR CALIBRATION FACILITY AT BESSY

As already mentioned, the essential prerequisite for the determination of $W(h\nu)$ from the spectral responsivity of photodiodes is the availability of accurate detectors. We describe in this section our experimental setup for the accurate measurement of the spectral responsivity.

In combination with power-stabilized lasers, radiant power of the order of 1 mW can be measured with a CESR with a relative uncertainty below 0.01%.[28–30] The operation principle of a CESR, see Fig. 1, is that an absorber trans-

Downloaded 19 Jun 2003 to 192.135.10.241. Redistribution subject to AIP license or copyright, see http://ojps.aip.org/japo/japcr.jsp

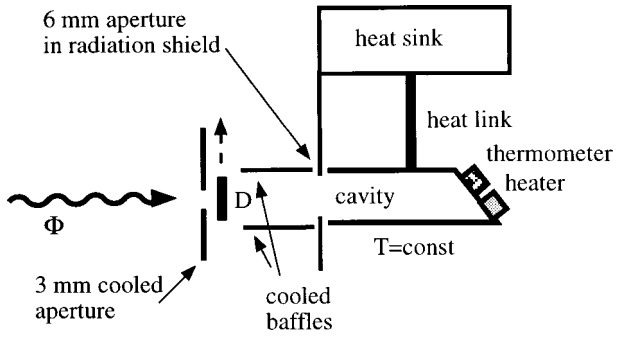

FIG. 1. Schematic drawing of the cryogenic electrical substitution radiometer. The cavity absorber is connected to a heat sink at liquid helium temperature. The cavity temperature T is kept at a constant value by an electrical heater. The radiant power Φ equals the difference in electrical heater power required to maintain $T=\text{const}$ with (shutter open) and without (shutter closed) synchrotron radiation. The 3 mm cooled aperture is used to suppress the scattered-light tails of the photon beam and, together with the cooled baffles, the infrared background radiation. The shutter (not shown in the figure) is placed in front of the monochromator, so that it does not influence the infrared background radiation at the CESR. The distance between the aperture and the radiometer is about 1 m, see Fig. 2. The diode D is shown in the measurement position. It is removed upwards from the beam for the radiant power measurement.

forms the incident radiant power Φ into a heat flow directed through a heat link to a heat sink kept at a constant temperature. When the CESR is operated in the dynamic substitution mode, the absorber temperature T is kept constant as well, and provided the absorber geometry ensures an absorptance sufficiently close to unity, the radiant power equals the change in electrical heater power required for keeping the absorber temperature at a constant value when the radiation shutter is opened. If absorber and heat sink are operated at liquid helium temperatures (CESR), the influence of thermometer noise is reduced, lead resistances are avoided by the use of superconducting leads, and a fast response is achievable as is a high responsivity. Moreover, nonequivalence issues between radiant and electrical heating are minimized. A critical issue of non-equivalence between radiation and electrical heating for room temperature radiometers is the heat transport by radiation, which depends on the temperature distribution at the absorber. It is often difficult to achieve equal temperature distribution for radiation and electrical heating due to, e.g., inhomogeneous illumination or slight differences in the size and position of the photon beam and the electrical heater. At liquid helium temperatures, the radiation does not contribute to the heat transport, so that these problems can be avoided.

A CESR designed for use with synchrotron radiation[19,31] was used for the measurements presented here. Cooled baffle systems in front of the radiometer reduce the thermal background load. The last aperture in front of the cavity, 6 mm in diameter, defines the sensitive area of the CESR. A total heating power of 12 μW was employed, and the corresponding absorber temperature of 5.8 K was kept constant to better than ± 20 μK.[31] The electrical power fluctuations caused by the temperature controller turned out to be the dominant source of uncertainty in the measurement of a radiant power of up to 2 μW (Table I). For a radiant power of 5 μW, the uncertainty of the cavity absorptance and the nonequivalence limit the accuracy achievable.

TABLE I. Relative uncertainty of the radiant power Φ measured with the CESR, see Ref. 19, and the additional contributions to be taken into account for the measurement of the spectral responsivity of photodiodes.

	Relative uncertainty at a radiant power value of			
Source of uncertainty	0.2 μW	1 μW	2 μW	5 μW
Radiant power (CESR)	1%	0.4%	0.3%	0.3%
Radiant power normalization		0.07%		
Diode current measurement		0.1%		
1% stray light and higher diffraction orders		0.2%		
Total (spectral responsivity)	1%	0.45%	0.4%	0.4%

The cavity absorptance was shown to be higher than 99.9% (Ref. 31) for UV radiation. In the soft x-ray region, the amount of backscattered or fluorescence radiation was measured at an incident photon flux of 1.5×10^{11} s^{-1} at 120 eV photon energy using a detector with a solid angle of $2\pi\,(1\times10^{-4})$ sr and a detection efficiency of about 2%. The total count rate including background was 150 s^{-1}, setting a relative upper limit of 5×10^{-4} to any scattering and fluorescence losses. The 120 eV photon energy was chosen, since the highest photon flux was available at this energy and the effects of backscattering were expected to be more important at lower photon energies. The same measurement at 900 eV photon energy yielded, however, about the same ratio of backscattered photons. This indicates that the measurement may be dominated by background effects such as counting photo-desorbed ions. Another possible energy loss process is the escape of electrons. We measured a ratio of 3×10^{-5} electrons/photon at 100 eV photon energy and 2×10^{-4} at 1 keV, setting an upper limit of 2×10^{-4} for this loss process. The absorptance thus is better than 99.93%.

Another critical effect is the possible loss of radiant power to radiation damages, see Ref. 19. By a direct comparison of the CESR to the primary source standard BESSY,[22] as announced in Ref. 19, this loss was preliminarily determined. It amounts to 0.006 ± 0.003. A detailed presentation of these investigations will be published elsewhere. The results presented here are corrected for this effect. The value for W differs therefore slightly (well within the 1σ uncertainty) from the previously published value.[23]

A soft x-ray beamline at the PTB's Radiometry Laboratory at BESSY was designed for detector calibration with monochromatized radiation in the spectral range from 40 to 1500 eV,[32] Fig. 2. Using the 200 μm wide exit slit, it provides a radiant power of a few μW, and a bandwidth defined by the slit. Other contributions to the bandwidth originating from optical aberrations and slope errors of the optical surfaces can be neglected in comparison to this exit slit. Therefore the spectral distribution can be approximated by a rectangle with a width varying between 0.05 eV at 50 eV photon energy and 9 eV at 1500 eV energy of the photons. The bandwidth is proportional to $h\nu^{3/2}$, as seen in Fig. 6 of Ref. 32. The influence of the width of the photon spectrum on the measurement of s is small because s is practically constant

Downloaded 19 Jun 2003 to 192.135.10.241. Redistribution subject to AIP license or copyright, see http://ojps.aip.org/japo/japcr.jsp

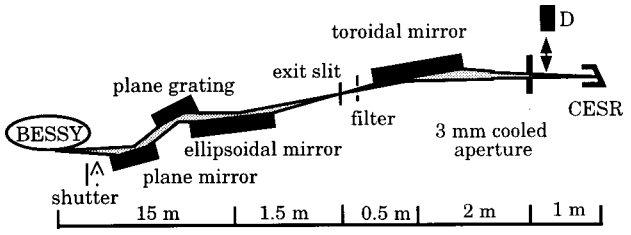

FIG. 2. Schematic drawing of the soft x-ray detector calibration facility of PTB at BESSY (side view). It consists of a plane grating monochromator, a toroidal collimating mirror to provide a low-divergence photon beam, and the CESR. A shutter is placed in front of the monochromator. The setup of CESR and photodiode *D* is shown in detail in Fig. 1. Details of the monochromator are given in Ref. 32.

within the bandwidth. The spectrum of the radiation outside the monochromator bandpass was determined using transmission gratings (below 200 eV) and energy-dispersive Si(Li) detectors (above 200 eV). The contribution of stray light and higher diffraction orders of the plane grating is below 1%.[32] Figure 3 shows the radiant power for a stored electron current of 500 mA under normal operating conditions. The typical stored electron current at BESSY varies between 800 and 300 mA.

The time structure of the synchrotron radiation at BESSY is approximately 200 ps bunches with 2 ns intervals. The ratio of peak flux to average flux thus is about 10:1. For the operation of the CESR, this is no restriction, since the thermal time constant of the detector is of the order of 100 s, therefore no difference from continuous irradiation can be detected. For other detectors such as, e.g., photodiodes for which the detected signal (ionization) is created at a time scale comparable to or shorter than the bunch length, the peak flux must be kept well within the linear dynamic range of the detector. Otherwise, the following time averaging in a slow current amplifier would yield incorrect results. The photodiodes used here have a linear response up to a detector output of about 1 mA, while the typical output during the measurements was only of the order of 1 μA.

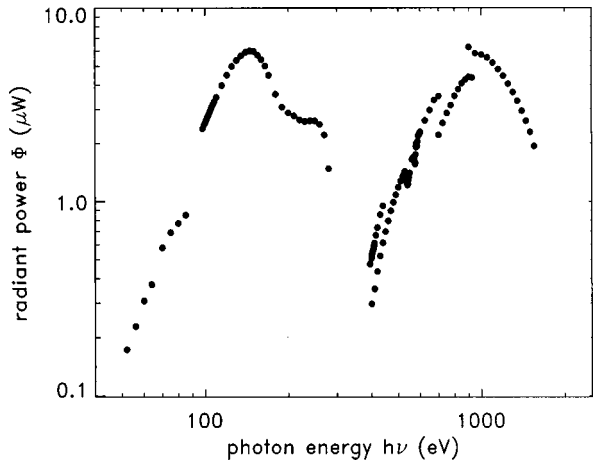

FIG. 3. Radiant power Φ leaving the 3 mm cooled aperture of the soft x-ray beamline of Fig. 2. It is given for a stored electron current of 500 mA. The discontinuities in the radiant power are due to the different filters used to suppress higher diffraction orders of the monochromator grating.

Another topic to be considered is the stochastic nature of the photon emission process. The typical photon flux used for measurements with the CESR is of the order of 10^{12} s^{-1}. The measuring time with the CESR is of the order of 100 s, corresponding to an accumulation of 10^{14} photons. The Poisson statistics thus yield a fluctuation of the order of 10^7 photons, 10^{-7} in relative terms. This can be neglected considering the fluctuations introduced by the temperature control circuit of the CESR.

As the stored electron current monotonically decreases with time, so does the radiant power, and a comparison between two detectors is possible only if the radiant power can be scaled with an independent monitor signal. We used the stored electron current as the monitoring signal. A relative standard deviation of 0.07% of the radiant power normalized to the stored electron current at a radiant power level of about 5 μW was measured.[33] Since the uncertainties of the current measurement are included in this standard deviation, we do not additionally account for the uncertainty of the stored electron current measurement in the compilation of the measurement uncertainties, Table I.

III. INVESTIGATION OF THE SPECTRAL RESPONSIVITY OF SILICON PHOTODIODES FOR THE DETERMINATION OF $W(h\nu)$

W can be determined from the spectral responsivity of photodiodes, $W=es_r/s$. The dimensionless factor s_r is defined as the ratio of the spectral responsivity of the diode under test to the spectral responsivity of an ''ideal'' diode ($s=e/W$) which is not affected by any loss process, such as reflection, absorption in insensitive surface layers (passivating oxide), escape of fluorescence radiation or electrons or the recombination of electron-hole pairs before they are collected at the electrodes. s_r will be referred to as relative responsivity hereafter. Calculation and measurement of s_r are discussed in the following sections.

A. Measurement of the spectral responsivity of silicon photodiodes

The detectors used are 10 mm by 10 mm silicon photodiodes with a shallow *n*-conducting front region on top of a *p*-type epitaxial layer 35 μm in thickness on a 200 μm p^+ substrate,[34] passivated with a nitrided oxide (4.3 nm thick) for high radiation hardness.[35]

The spectral responsivity of a total of 17 diodes was measured at room temperature at the PTB's soft x-ray detector calibration facility, Fig. 2. The current induced in the diode by the radiation incident on it was measured with a Keithley 617 electrometer. The radiant power was measured using the CESR and normalized to the stored electron current in BESSY. The bias voltage at the diode was below 0.1 mV, the input burden voltage of the electrometer. The electrometer was calibrated with an uncertainty of 0.1% using a standard resistor and a voltmeter with a relative measurement uncertainty of less than 10^{-4}. The time constant of the current amplifier was 300 ms and about ten individual measurements were averaged at each photon energy. The relative variance of the ten measurements was of the order of 10^{-4}. The fundamental limitation by the stochastic nature of the

Downloaded 19 Jun 2003 to 192.135.10.241. Redistribution subject to AIP license or copyright, see http://ojps.aip.org/japo/japcr.jsp

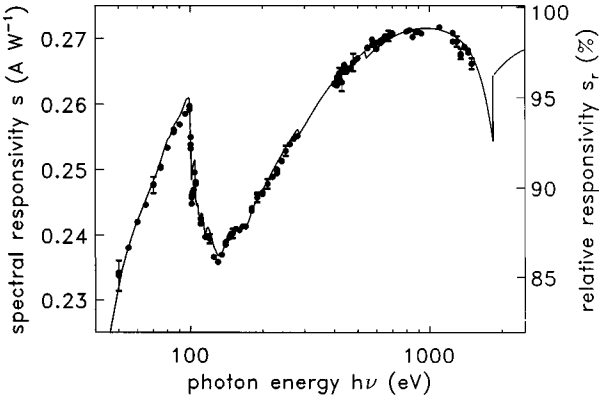

FIG. 4. Spectral responsivity s (symbols, left axis) of an n-on-p silicon photodiode measured against the CESR and relative responsivity s_r (solid line, right axis) calculated using Eq. (2), with the parameters determined from the angle dependence measurement, Fig. 5. Some typical uncertainties are shown.

photon emission can be estimated in the same way as for the CESR to be about 10^{-6} using an effective integration time of the order of 1 s.

The CESR was aligned behind a cooled aperture 3 mm in diameter and kept fixed during the measurements. The diode was mounted on a linear feedthrough and placed behind the same aperture for the measurement of the photocurrent, see Fig. 1. Since the photon beam did not cover either detector completely, uncertainties in position need not be taken into account. The spectral responsivity measured is shown in Fig. 4. It varies by less than 15% over the spectral range investigated here. Since $s(h\nu)$ is almost constant, the influence of stray light and higher diffraction orders (about 1%) is below 0.2%. The spectral responsivity of the same diode measured repeatedly over several weeks varied by less than 0.2%.[33] The uncertainties of measurements at different radiant power values are summarized in Table I. The typical relative uncertainty was 0.4% (1σ) for a measurement at a radiant power above 1 μW. The data at the lowest photon energies were obtained at a radiant power of about 0.2 μW, see Fig. 3, so that the relative uncertainty was up to 1% in that spectral range.

B. Description of the relative responsivity of silicon photodiodes

The determination of $W=es_r/s$ requires a method to determine s_r. s_r can be obtained by integration over the diode thickness of the probability that an incident photon penetrates into the diode and is absorbed at a certain depth x from the diode surface times the probability that the energy of that photon will be absorbed in the sensitive region of the diode times the collection efficiency for the free charge carriers resulting from the ionization process:

$$s_r(h\nu)=[1-\rho(h\nu)]\int_{-d_{\mathrm{ox}}}^{d} e^{-\overline{\mu}(x)x}\mu_p(h\nu,x)\zeta(h\nu,x)dx \tag{1}$$

with

$$\overline{\mu}(x)=\frac{1}{d_{\mathrm{ox}}+x}\int_{-d_{\mathrm{ox}}}^{x}\mu(h\nu,x')dx'.$$

d_{ox} is the thickness of the oxide. ρ is the reflectance, μ the linear attenuation coefficient, μ_p the photoabsorption coefficient, and $\zeta(h\nu,x)$ the collection efficiency for charge carriers created by the absorption of a photon of energy $h\nu$ at position x. $\zeta(h\nu,x)$ accounts for possible losses by the escape of fluorescence photons as well as the escape of electrons, losses during the thermalization of the electrons and, finally, charge carrier recombination losses. Other loss processes were not considered here. Atomic dislocations, which are important for high-energy particle detection, are impossible due to momentum conservation. Other chemical modifications are impossible in pure silicon as there are only silicon atoms which can only be dislocated, and the concentration of impurities, which are not located at well-defined positions (as the donors and acceptors) and thus possibly subject to metastable excitations, must be extremely low to achieve the long minority carrier lifetimes needed for diode operation. In the oxide, however, chemical modifications are possible. A disturbing effect is, e.g., the release of hydrogen which passivates dangling bonds at the interface, increasing the recombination velocity at the silicon-oxide interface. The diodes used here were selected for sufficient stability under irradiation, so that this effect can be neglected.

The integration range is the total diode thickness d because a shallow region of the field-free substrate on the back side of the diode may contribute to the signal by charge diffusion into the depletion region. It appears, however, that d can be set equal to the thickness of the low doped epitaxial layer (Appendix B).

Due to the high attenuation coefficient for photons in the soft x-ray spectral region, the magnitude of s_r is mainly determined by the photoabsorption in the oxide and by charge recombination effects at the oxide-silicon interface. We therefore focused on the description of the front side of the diode and adapted the diffusion model that was developed for solar cells[36] to describe the back side region. For normal incident radiation, s_r is obtained as

$$s_r/(1-\rho)=(1-\alpha_{\mathrm{ox}})[1-\epsilon_f(r_i,l_{\mathrm{th}})-\epsilon_b(d_d,d,\epsilon_{\mathrm{end}}) -\epsilon_p-\epsilon_s]+\epsilon_{\mathrm{ox}} \tag{2}$$

with

$$\alpha_{\mathrm{ox}}=1-\exp[-\overline{\mu}(0)d_{\mathrm{ox}}]$$

α_{ox} is the absorptance of the oxide. The terms $\epsilon_i(i=f,b,p,s,\mathrm{ox})$ represent the integrals of the corresponding contributions to $\zeta(h\nu,x)$ in Eq. (1). ϵ_f describes the recombination loss at the oxide interface, parametrized by a charge carrier reflection probability at the interface, r_i, and a thermalization length l_{th}, for details, see Appendix B and Fig. 1 in Ref. 26. The photon transmission loss ϵ_b is a function of depletion depth d_d, the thickness of the epitaxial layer d, and the collection efficiency at the bottom of the epitaxial layer ϵ_{end}, for details, see Appendix B. ϵ_p and ϵ_s are the photon

Downloaded 19 Jun 2003 to 192.135.10.241. Redistribution subject to AIP license or copyright, see http://ojps.aip.org/japo/japcr.jsp

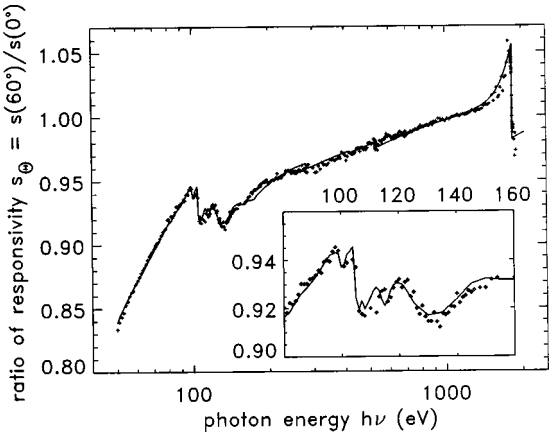

FIG. 5. Ratio s_Θ of the spectral responsivity of an *n*-on-*p* diode at 60° to the responsivity for normal incident radiation (crosses) and calculation with the best fit parameters (solid line). The relative uncertainty of measurement is about 0.2%.

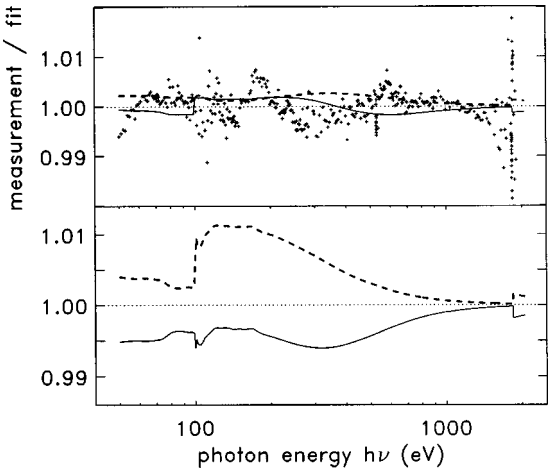

FIG. 6. Upper part: Ratio of measured to fitted values for s_Θ (crosses). Ratios are also shown for a calculation in which l_{th} for ϵ_f [Eq. (2)] was increased from 170 to 220 nm (solid line) and *a* calculation in which r_i was increased from 84% to 86.5% (dashed line). Lower part: Ratio of two calculations for s_r, using the same modified values for l_{th} and r_i, which have been used for the calculation of s_Θ in the upper part, to the function s_r calculated with the fitted parameters for s_Θ. The line styles are the same as in the upper part. The dotted line is shown to guide the eye.

and electron escape losses, while ϵ_{ox} is the contribution of electrons originating from the oxide, see Appendix C.

In the case of nonnormal incidence of the radiation, the attenuation coefficient for the incoming radiation must be multiplied by a factor of $1/\cos(\Theta)$ and for photon energies below 100 eV the effect of refraction must be taken into account.

The oxide transmittance $\tau_{ox}=(1-\rho)(1-\alpha_{ox})$ is the dominant contribution in Eq. (2), see Fig. 11. The data used for the oxide attenuation coefficient μ_{ox} are therefore of crucial importance. In the 50 to 200 eV spectral range, we determined therefore the oxide thickness $d_{ox}=4.3$ nm and μ_{ox} from reflection measurements, see Appendix A and Ref. 37. Above 200 eV, μ_{ox} was calculated from the atomic scattering factors of Henke *et al.*[38]

The next dominant contribution to s_r is the recombination loss ϵ_f, see lower part of Fig. 12. The remaining terms are only small corrections. ϵ_s and ϵ_{ox} contribute about 1% and are nearly equal above 100 eV. Below 100 eV, ϵ_s is negligible while ϵ_{ox} contributes up to 2% at 50 eV, see Fig. 13. ϵ_p is significant only directly above the silicon *K* edge.

C. Experimental determination of the relative responsivity

The ratio of the measured response for radiation, incident at 60° to the normal, to the response to normally incident radiation, $s_\Theta=s(60°)/s(0°)$, is used to determine s_r as described in Ref. 20. s_Θ is shown in Fig. 5 with the best fit of Eq. (2), using d_d, d, ϵ_{end}, l_{th}, and r_i as fit parameters. Note that there is no cross correlation between the parameters l_{th} and r_i for ϵ_f on the one side and d, d_d and ϵ_{end} for ϵ_b on the other, see Appendix B. This increases the significance of the fitted parameters. Carbon surface contamination, identified by an absorption edge at 280 eV and confirmed by the reflection measurements, was also taken into account. The best fit parameters are a 0.5 nm carbon layer, $d_d=2$ μm, $d=47$ μm, and $\epsilon_{end}=85\%$ and $l_{th}=170$ nm and $r_i=84\%$.

The agreement between fit and measurement for photon energies above 1 keV is not perfect. This may be due to the approximations in the model for ϵ_b, which are discussed in Appendix B. The contribution of ϵ_b decreases, however, with decreasing photon energy and accounts only for 0.35% at 1 keV so that there is no influence of ϵ_b below 1 keV. The relative measurement uncertainty of s_Θ is about 0.2%. This yields a reduced $\chi^2=1.35$ for the fit of the 290 measurement points in the energy range below 1.2 keV, Fig. 5, suggesting some residual systematic deviations of the model, which are seen in Fig. 6, showing the ratio between measurement and fit. The absorption fine structure in the energy range between 100 and 250 eV and that at the oxygen *K* edge at about 530 eV do not fit perfectly. The most critical parameters of the fit are r_i and l_{th}, because s_r is much more sensitive to changes of these parameters than s_Θ, and changes of s_r for photon energies around the silicon *L* edge must be well separated from possible changes of *W*. The effect of an increase in either r_i by 2.5% or l_{th} by 50 nm on s_r and s_Θ is shown in Fig. 6. Although the changes of s_Θ are within the scatter of the measured values at most of the photon energies, the corresponding χ^2 are 1.74 and 1.69, respectively, i.e., the deviation from unity is about two times that of the best fit value. When these are used as limiting values, the resulting uncertainty of s_r is 0.5% for energies above 500 eV and 1% below this value, see lower part of Fig. 6.

IV. EXPERIMENTAL AND THEORETICAL VALUES FOR $W(h\nu)$

A. Experimental values for $W(h\nu)$

In Fig. 4, s and s_r (right axis) are shown in comparison. It is already obvious from Fig. 4 that s and s_r differ only by a factor (e/W) which is constant within the measurement uncertainties. The values of *W* determined from s_r and s at

Downloaded 19 Jun 2003 to 192.135.10.241. Redistribution subject to AIP license or copyright, see http://ojps.aip.org/japo/japcr.jsp

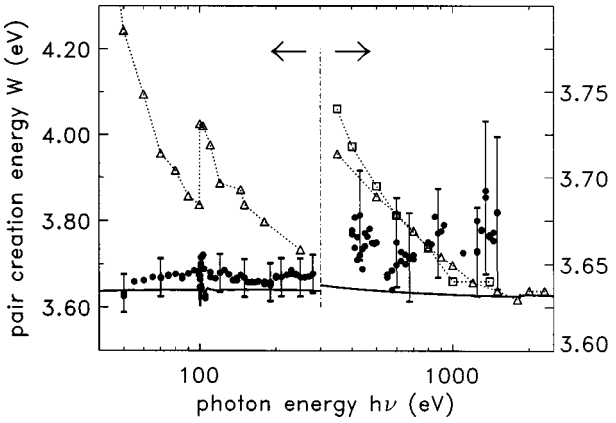

FIG. 7. Mean energy W required for the creation of an electron-hole pair, determined from s_r and s (filled circles). The theoretical data of Ref. 14 (triangles) and experimental data of Ref. 16 (squares) are scaled from 170 K to room temperature using the temperature dependence given in Ref. 14. The solid line is our calculation of W. The right half is plotted on an expanded scale. The dotted lines are shown to guide the eye.

room temperature are shown as points in Fig. 7. The relative uncertainty varies from 0.7% to 1.4%, Table II.

The average value of all experimental data in Fig. 7 is $W=3.66$ eV with a standard deviation of 0.016 eV. The structures which appear around 100 eV are more likely due to variations of s_r from the fitted values caused by the absorption fine structures of the nitrided oxide and the silicon and probably are not due to variations of W. The individual results, which have uncertainties of typically 0.05 eV, see Table II, confirm the constant value of W within this uncertainty.

The standard deviation of the experimental values of 0.016 eV consists of two parts, possible real variations of W as a function of the photon energy and the deviations of s_r from the fitted values. The measurement uncertainty for the spectral responsivity of the diodes with the CESR (0.4%, Table I) is dominated by systematic contributions which do not depend on the photon energy[19] and thus do not average out in the calculation of the mean value. This uncertainty is therefore added to the standard deviation of the experimental results and a mean value of $W=(3.66\pm0.03)$ eV is obtained for the soft x-ray spectral range from 50 to 1500 eV. Assuming a constant value for W, which is verified by our calculation of W, this reduced uncertainty can also be applied to each individual photon energy.

TABLE II. Contributions to the relative measurement uncertainty of the mean electron-hole pair creation energy.

	Relative measurement uncertainty of W in the photon energy range:			
Uncertainty contribution	50–90 eV and 350–500 eV	90–250 eV	500 eV–1.2 keV	1.2–1.5 keV
Spectral responsivity	0.4%–1%	0.4%	0.4%	0.4%
Relative responsivity	1%	1%	0.5%	1%
Sum in quadrature	1.1%–1.4%	1.1%	0.7%	1.1%

B. Calculation of $W(h\nu)$

In this section, we present our approach to the calculation of the internal quantum yield η, which is related to W by $W=h\nu/\eta$. The generation of charge carriers can be divided into two steps. First, the absorption of the photon and the following relaxation of the excited atom, which yields the photoelectron and Auger and Coster-Kronig ''primary electrons'' and a corresponding number of holes in the valence band, ''primary holes.'' In the second step, all primary electrons and holes lose their kinetic energy, partially by phonon scattering with an energy loss of the order of 64 meV and partially by impact ionizations leading to the production of secondary electron-hole pairs.

The average number of secondary electron-hole pairs created by a primary electron or hole is a function $n_e(E)$ or $n_h(E)$ of the kinetic energy E of the initial electron or hole. It should therefore be noted that, for a photoabsorption from an inner shell, only the energy of the photoelectron depends on the photon energy, whereas the energies of all other primary electrons and all primary holes depend exclusively on the vacancy created by the photoionization. If p^j_{ex} and p^j_{hx} denote the energy distribution functions of the primary electrons and holes, respectively, that are produced in the atomic relaxation process j following photoabsorption in the atomic subshell x with binding energy E_x, the resulting average number of electron hole pairs, η^j_x is given by

$$\eta^j_x(h\nu)=1+n^j_{0x}+n_e(h\nu-E_x)+\sum_{i=1}^{n^j_{0x}}\left[\int_0^{\infty}p^j_{ex}(i,E)n_e(E)dE\right]+\sum_{i=1}^{n^j_{0x}+1}\left[\int_0^{E_V}p^j_{hx}(i,E)n_h(E)dE\right]. \quad (3)$$

The ''1'' stands for the photoelectron, n^j_{0x} is the number of Auger and Coster-Kronig electrons created in the atomic relaxation process, $n_e(h\nu-E_x)$ is the number of pairs created by the photoelectron, which determines the photon energy dependence of η^j_x. η_x, the quantum yield for subshell x, is obtained as: $\eta_x=\Sigma_j\eta^j_x p_j$, with the probabilities p_j of the different relaxation channels j.

For photoabsorption from the valence band, the energy of the primary vacancy and thus the energy of the photoelectron is not sharply defined, as the valence band has a finite width of $E_V=12$ eV. For photons with energies $h\nu\gg E_V$, the energy distribution of the holes does not depend strongly on the photon energy, so it can be approximated by a fixed energy distribution function similar to that of primary vacancies resulting from the inner shell relaxation processes.

The average number of electron-hole pairs for a given photon energy is obtained by summation over all subshells x that can be excited, weighted with the partial photoabsorption cross sections μ_x of each subshell:

$$\eta(h\nu)=\sum_x\frac{\mu_x(h\nu)}{\mu(h\nu)}\eta_x. \quad (4)$$

Downloaded 19 Jun 2003 to 192.135.10.241. Redistribution subject to AIP license or copyright, see http://ojps.aip.org/japo/japcr.jsp

TABLE III. Compilation of the atomic relaxation processes included in the calculation of n_{0x}^{j}. Only the dominant transitions up to a total transition rate of 90% were used and their sum was renormalized to 1.

Excited subshell (x)	Transition chain (j)	Probability	n_{0x}^{j}
Valence band	photoelectron only	1	0
L_3 shell	L_3MM	1	1
L_2 shell	L_2MM	1	1
L_1 shell	$L_1L_3M+L_3MM$	1	2
K shell	$KL_1L_1+2L_1L_3M+2L_3MM$	0.21	5
	$KL_1L_3+L_1L_3M+2L_3MM$	0.425	4
	$KL_3L_3+2L_3MM$	0.255	3
	$KL_1M+L_1L_3M+L_3MM$	0.11	3

An effect of the x-ray absorption fine structure of μ_x on η would result only if the η_x of the different subshells differed significantly. We will see that the η_x are nearly equal for all subshells so that any absorption fine structure effects on η, as claimed by Owens *et al.*,[39] are very unlikely to appear. On the other hand, as the photoabsorption cross section for the lowest atomic level that can be excited usually dominates the total photoabsorption cross section, it follows from Eqs. (3) and (4) that the variation of η above an absorption edge is mainly defined by the number of impact ionizations by the photoelectron.

For $n_e(E)$ and $n_h(E)$, we use the same function. It is given by the number of impact ionizations by energetic charge carriers $n(E)$ as deduced by Alig,[6,7] which was also used by Geist and Wang.[5] In the kinetic energy range from 1.8 to 3.5 eV, the data are deduced from the single ionization probability given in Fig. 7 of Ref. 6. In the energy range from 3.5 to 100 eV, the data are read from Fig. 2 of Ref. 7, and above 100 eV approximated by $n(E)=(E-1.6\ \mathrm{eV})/3.63\ \mathrm{eV}$. Direct measurements of charge generation by hot carriers with energies of a few eV injected into the channel of a metal–oxide-semiconductor field effect transistor (MOSFET)[40] agree well with the results of Alig in the kinetic energy range from 1.5 to 5 eV. New evaluations of the basic equations for energetic electrons moving in the silicon band structure[41,42] did not show differences from Refs. 6, 7 except for electron energies at the ionization threshold. Refs. 6, 7 suggest a threshold at 1.8 eV, while according to Ref. 42 the strong wave-vector dependence of the threshold leads to a wave-vector-averaged ionization probability that decreases exponentially from 2 eV to the band gap energy $E_g=1.12$ eV. The wave-vector dependence of the ionization threshold is significant only for resonant photoabsorption in the UV spectral range which yields a high probability of initial states with a low ionization threshold.[8]

n_{0x}^{j} was calculated with the Auger and Coster-Kronig transition rates which were used in the Monte Carlo simulation of Fraser *et al.*, see Table III. The energy distribution functions $p_{ex}^{j}(i,E)$ and $p_{hx}^{j}(i,E)$ were approximated by $p(E)=1/E_V$ for holes, Coster-Kronig electrons, KLM Auger electrons, and valence band photoelectrons whose kinetic energy varies within a range of the width E_V. For xMM Auger electrons, $p(E)=1-|E_x-2E_g-E_V-E|/E_V$ was used in the energy range $E_x-2E_g-2E_V<E<E_x-2E_g$, with $x=K,L_1,L_2,L_3$.

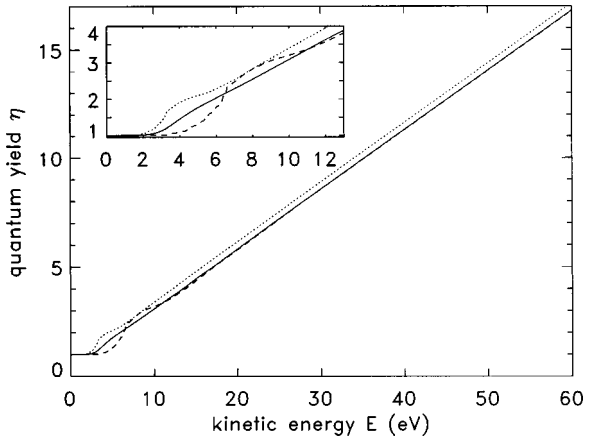

FIG. 8. Calculation of quantum yield η for three cases, see Eq. (5). η represents the number of secondary electron-hole pairs produced by one primary electron-hole pair with total kinetic energy E. The solid line shows η_V, the dashed line η_1, and the dotted line η_2. The inset shows the low-energy range in detail.

To estimate whether this rather simple approximation of the energy distribution functions is sufficient, we calculated the quantum yield η_V for photoabsorption in the valence band, resulting in an electron and hole of energies E_e and E_h, respectively, with $E_e+E_h=E=h\nu-E_g$,

$$\eta_V-1=1/E_V\left[\int_{E-E_V}^{E}n(E')dE'+\int_{0}^{E_v}n(E')dE'\right]. \quad (5)$$

η_V is shown in Fig. 8 together with two limiting cases for comparison. First, $\eta_1-1=n(E)$, i.e., the total kinetic energy is transferred to the photoelectron. Second, $\eta_2-1=2n(E/2)$ for $E<2E_V$ and $\eta_2-1=n(E-E_V)+n(E_V)$ for $E>2E_V$, respectively, i.e., where possible, the energy is split into equal parts between electron and hole, or, for higher photon energies, the maximum energy E_V is transferred to the hole. η_1 and η_2 were used as upper and lower limits for η in the UV photon energy range.[5]

The differences $\Delta\eta_x=\eta_x-\eta_V$, $x=1,2$ are below 0.5 for all energies and constant for kinetic energies above 15 eV. The high-energy limit of $\Delta\eta_1$ is 0.35. η_2 and η_V, on the other hand, are nearly equal above 15 eV ($\Delta\eta_2=-0.02$). Both η_V and η_2 include an energy transfer to the primary hole. Using the asymptotic approximation $n(E)=(E-1.6\ \mathrm{eV}/3.63\ \mathrm{eV})$, splitting the energy between two particles yields an energy loss of 1.6 eV. The energy distribution of the hole thus seems to have only a minor influence as long as the hole has non-zero energy, while the assumption that the complete kinetic energy is transferred to the electron leads to a significant overestimation of η.

The results of a calculation of W for silicon based on Eq. (4) are shown in Fig. 9. The region around the $L_{2,3}$ edge is represented in the inset. There is no significant discontinuity at that energy; only an oscillation of the order of 1% is observed in the photon energy range up to 10 eV above the edge, caused by the nonmonotonous variation of the average number of impact ionizations by the photoelectron. Besides this oscillation, the result is $W=(3.640\pm0.003)$ eV between 50 and 300 eV, and above 300 eV, it slowly decreases to 3.632 eV at 2.5 keV photon energy. Below 50 eV, our model

Downloaded 19 Jun 2003 to 192.135.10.241. Redistribution subject to AIP license or copyright, see http://ojps.aip.org/japo/japcr.jsp

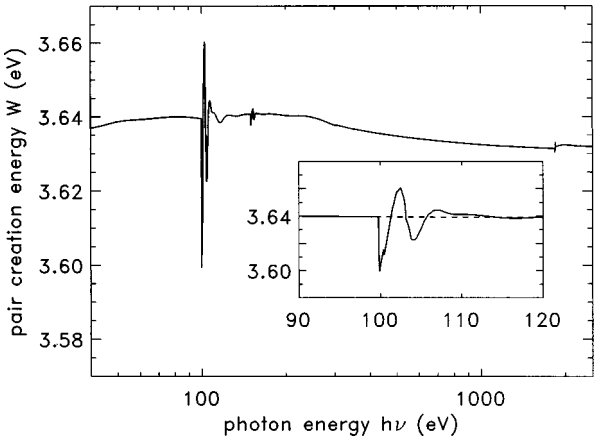

FIG. 9. Calculation of W for silicon with Eq. (4). The inset shows an expanded view of the region of the $L_{2,3}$ edge. Also shown is η_V in the energy range above the L edge by the dashed line in the inset.

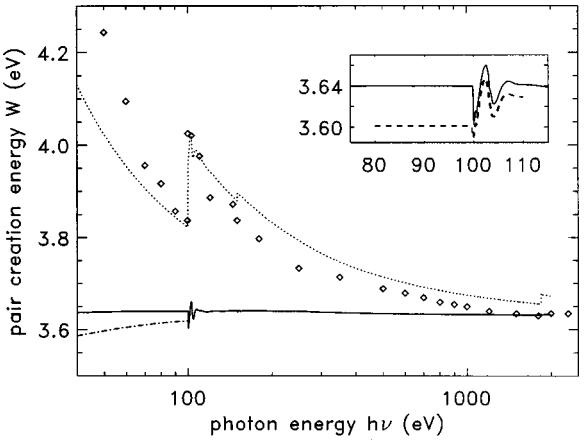

FIG. 10. Comparison of our calculation (solid line) with the calculation of Fraser *et al.* (diamonds). Also shown is our calculation in which the contribution of the holes is neglected (dotted line). The dash-dotted line shows W calculated using the average of η_1 and η_2 which was used as an approximation of η for photon energies below 100 eV in Ref. 13. The dashed line in the inset shows the data from Ref. 13 in comparison to our calculation.

suggests that W remains constant down to photon energies as low as 20 eV. For lower photon energies, the band structure of Si has to be considered to determine the initial energy of the photoelectron. This is discussed in Ref. 5.

C. Comparison of the experimental and theoretical values for $W(h\nu)$

The calculation of W presented in the previous section and the experimental results provide a constant value of W in the soft x-ray region. Although the calculated values are within the 1σ uncertainties of the experimental values for nearly all photon energies, they appear to be systematically low. Our experimental values are closer to $W=3.68$ eV obtained for the soft x-ray range by Krumrey and Tegeler[20,21] and for high-energy β and γ rays in Refs. 2 and 4. Our calculation, on the other hand, is based on the results of Alig, who used a value of $W=3.63$ eV, from, e.g., Ref. 3, to adjust the ratio between phonon and ionization scattering which defines the asymptotic value of W. The difference is therefore easy to explain and some more accurate measurements of W could probably be used to reevaluate the calculations of Alig with a new value of the ratio of phonon to ionization scattering.

The result of a constant W is different from the result in Fig. 7 of Fraser *et al.*[14] In our Fig. 10 our calculation is shown in comparison with the recent calculations of Fraser *et al.* and Geist.[13] The theoretical model of Geist[13] is below the silicon $L_{2,3}$ edge just within the experimental uncertainties of the individual measurement points, see error bars in Fig. 7, but it is systematically low. He approximated η_V by $(\eta_1+\eta_2)/2$, yielding a lower pair creation energy below the silicon L edge, as η_1 significantly overestimates η_V which is close to η_2.

The atomic relaxation process was ignored completely, and the mean number n_L of electron-hole pairs created by a vacancy in the L shell was assumed to be equal to $n(E_L)=26.75$, the number of electron-hole pairs created by an electron of the kinetic energy $E_L=E_{L3}-E_g$ in Ref. 13. This turns out to be sufficiently accurate because a proper calculation using Eq. (3) yields $n_L=\eta_L(E_{L3})-1=26.79$. The difference between the total number of impact ionizations caused by the *LMM* Auger electron plus the two holes created in the Auger process, and the number of ionizations caused by an electron of the L-shell energy thus is negligible.

For comparison, it should be noted that Geist also used the values of Alig for his calculation and the experimental results from the CCDs[16] were normalized at the highest photon energies to the asymptotic value of 3.63 eV.

The equivalence of the quantum yield for the *LMM* Auger electron and the holes on one side and the quantum yield for an electron of the L-shell energy on the other is the reason why W does not show a stepped variation at the $L_{2,3}$ edge. The same behavior can be derived for the K edge, where an additional *KLL* Auger process takes place. The main effect at an absorption edge is that additional Auger or Coster-Kronig transitions occur, resulting in an increased number of primary electrons and holes, see Table III.

For gas ionization detectors, it actually turned out that the differently charged photoions cause the variations in the mean pair creation energy, because the ground-state energy of a multiply charged ion exceeds the energy of the corresponding number of singly charged ions. The impact ionization process of the energetic electrons, however, most probably produces singly charged ions. As the charge of the primary photoions increases when lower core levels are excited, the mean pair creation energy for gases increases at each absorption edge.[43]

Fraser *et al.* used a gas-like atomic structure of silicon with M shells instead of the valence band. Therefore, the arguments given for the pair creation energy in gases also hold for this simulation and explain the variations at the edges. Fraser *et al.* simulated the slowing down of the electrons using cross sections for plasmon, electron, and phonon scattering. These cross sections, Ref. 44, are extracted from the energy spectrum of ^{31}Si β rays with a maximum initial energy of 1480 keV, escaping from neutron-activated silicon wafers. The measured energy spectrum was corrected for the effects of the silicon surface barrier. This correction starts being significant around 1 keV electron energy and increases

Downloaded 19 Jun 2003 to 192.135.10.241. Redistribution subject to AIP license or copyright, see http://ojps.aip.org/japo/japcr.jsp

to a factor of 6 at 10 eV. In this study, the cross sections for low electron energies should, therefore, have a rather high uncertainty. The simulation of the electron impact ionizations by Fraser *et al.* seems, however, to be very close to our calculation on the basis of $n(E)$ from Refs. 6, 7, as a calculation using Eqs. (3) and (4), but without the ionization by the holes, last term in Eq. (3), agrees remarkably well with the data of Fraser *et al.*, our Fig. 10.

The explanation by Fraser and co-workers[24] for the near-edge fine structure of *W* observed in CCD measurements at the silicon *K* edge[39] is also based on a gas-like structure, as they argue that in the case of photoabsorption in the ''white line'' resonance, the silicon atom is not ionized but an electron is transferred from the *K* shell to unoccupied (atomic) states and thus no photoelectron is released, decreasing η by 1. In the case of solid-state silicon, however, all unoccupied states are situated in the conduction band, so the photoelectron is in any case a free electron in the conduction band.

Recent experimental data for *W* from a CCD[16] supporting the model of Fraser *et al.* possibly suffer from incomplete correction for recombination losses. Only the energy range above 300 eV from which the charge collection efficiency is difficult to determine was covered. At low photon energies, there was scarcely any event for which the full charge was collected so that the complete peak was shifted to lower energies, thus causing an apparent increase in *W*. Recent data for a CCD with practically ideal charge collection efficiency,[17] covering Al *L*, C *K*, O *K*, Al *K*, and Mn *K* fluorescence, are consistent with both a constant *W* and the model of Fraser *et al.* as the authors explicitly state. In Ref. 39, the peak position around the silicon *K* edge was fitted using a Gaussian so that the increase of the charge collection losses results in an increased shift of the peak to lower energies and thus in higher values for *W* above the *K* edge.

V. CONCLUSION

Our experimental data for the electron-hole pair creation energy in silicon, derived from the spectral responsivity of photodiodes, measured with a relative uncertainty of 0.4% at the PTB's soft x-ray detector calibration facility, result in a constant value of $W=(3.66\pm0.03)$ eV in the soft x-ray spectral region. This result, together with the theoretical calculation which also gave a constant value, is a significant step forward to an improved understanding of *W* for silicon. The slight constant offset between our measurements and the calculation is most probably due the data for the quantum yield of electrons used in our calculation. Further measurements of higher accuracy could help to improve these data.

Our results further reduce the photon energy range, where for silicon the transition from $\eta=1$ to $W=\text{const}$ occurs, to the range from about 3 eV to about 50 eV and lead to better understanding of the charge generation process in silicon photodetectors.

APPENDIX

Here we summarize some experimental results and calculations which add necessary information for the reproduction of our results, but have been skipped from the body of the paper because they are not essential for a first understanding.

The relative responsivity can be described by the oxide absorptance α_{ox} and reflectance ρ, discussed here in Sec. A, and the charge collection efficiency $\zeta(h\nu,x)$ introduced in Eq. (1) $\zeta(h\nu,x)$ can be written as the result of a convolution:

$$\zeta(h\nu,x)=\rho_0(h\nu,x,x')\otimes\rho_t(x',x'')\otimes c(x''). \tag{A1}$$

$\rho_0(h\nu,x,x')$ denotes the distribution of the hot charge carriers originating from the ionization process of the primary photo and Auger electrons emitted by an atom at position *x*, which was ionized by a photon of energy $h\nu$. These electrons thermalize by phonon scattering and the diffusion during this thermalization process is described by the distribution $\rho_t(x',x'')$. $c(x'')$ denotes the collection efficiency for thermal electrons. The escape of primary (photo- and Auger) electrons and fluorescence photons can be described in that formalism by a truncation of the distribution ρ_0 to the sensitive region of the diode, see Sec. C. In the second step the remaining part of ρ_0 is convoluted with ρ_t and *c*, see Sec. B.

The equations below will only be given for normal incident radiation. In the case of non-normal incidence of the radiation, the attenuation coefficient for the incoming radiation must be multiplied by a factor of $1/\cos(\Theta)$. The effect of refraction has been taken into account for photon energies below 100 eV in the calculation of α_{ox}.

A. Oxide absorptance

A comparison between the diodes with a nitrided oxide, as used here, and similar diodes with silicon dioxide passivation layer showed a significant difference in the fine structure in the oxide absorption above the silicon *L* edge. We used reflection measurements to determine the optical data of the nitrided oxide. The measurements covered the energy range from 50 to 200 eV and angles of incidence from 5° to 83° to the normal. The reflectance varied from about 0.7 (at 83° and 50 eV) to 10^{-5} (at 5° above 100 eV). The high dynamic range of the measurements and the wide range of incidence angles, which could be covered with a typical relative uncertainty of the reflectance of about 1%, allowed the optical constants of the oxide to be fitted with sufficiently low uncertainty. The details of the procedure are presented in Ref. 37.

A consistent fit could be achieved only by assuming a double-layer structure for the oxide. An SiON/SiO composition was used for the top and bottom layers 2 and 2.3 nm thick, respectively, to extrapolate the absorption coefficient using the atomic scattering factors of Henke *et al.*[38] The results for τ_{ox} in the 50 to 200 eV energy range are shown in Fig. 11. At low photon energies, our result is within the range of recent experimental data for SiO_2,[45,46] while above 105 eV the higher silicon content of the oxide increases the average absorptance. This has a significant impact on the ratio of τ_{ox} below and above 100 eV, so that an extrapolation of the diode responsivity across the silicon *L* edge would be wrong if the data from Refs. 45 and 46 were used. The assumption of a significant oxygen deficiency of the oxide is

Downloaded 19 Jun 2003 to 192.135.10.241. Redistribution subject to AIP license or copyright, see http://ojps.aip.org/japo/japcr.jsp

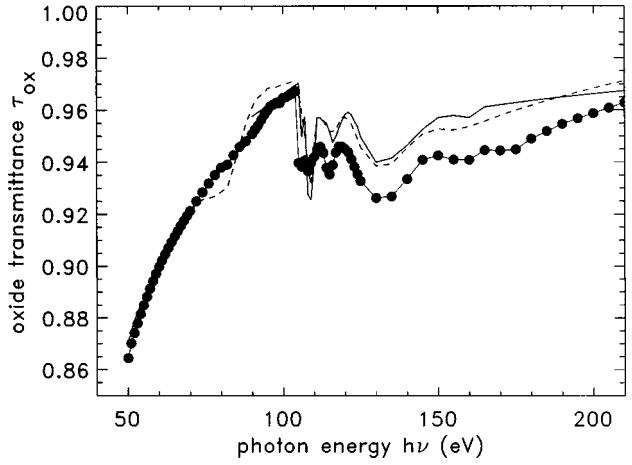

FIG. 11. Transmittance of the nitrided oxide. The points connected by a smooth line are our experimental data, the solid line represents the data of Tarrio and Schnatterly (Ref. 45) and the dashed those of Palik (Ref. 46).

confirmed by the low edge jump in τ_{ox} at the oxygen K edge at about 530 eV, see Figs. 5 and 6.

A similar double-layer model of the oxide passivation of a backside-thinned CCD was obtained by Morrisey *et al.*,[47] with a 2 nm SiO_2 layer on top of a 5.5 nm SiO layer, by fitting the normal incidence reflectance in the 4 to 12 eV spectral range, where SiO_2 and SiO can be identified by their different absorption coefficients.

B. Charge collection efficiency for non-thermal electrons

For photon energies of up to 2 keV, the range of the primary photo- and Auger electrons is short compared with the thermalization range l_{th} of about 200 nm. The width of the distribution ρ_0 is therefore much smaller than the width of ρ_t and the convolution of these distributions can be approximated by a spherical distribution of the thermalized electrons, $\rho_e(h\nu,x,x'')$. For the calculation presented here, it is approximated by a Gaussian distribution with a standard deviation $\sigma^2=l_{th}^2+R(h\nu)^2$, $R(h\nu)$ being the range of the primary electron of the highest kinetic energy.

Because of $R(h\nu)\ll l_{th}$ the very shallow region near the front silicon-oxide interface, where ρ_0 has to be truncated, can be neglected for the calculation of the recombination losses. The distribution $\rho_e(h\nu,x,x'')$ has therefore to be convoluted with the collection efficiency $c(x'')$ and the resulting $\zeta(h\nu,x)$ must be integrated over the sensitive layer of the diode.

For convenience, we divide $\zeta(h\nu,x)$ into two factors, namely, the charge collection efficiency determined by surface recombination, $\zeta_1(h\nu,x)$, and the part $\zeta_2(h\nu,x)$ determined by diffusion in the backside field-free region. For realistic diodes with not too shallow a depletion depth, ζ_1 and ζ_2 deviate from unity only in separate regions of the diode so that $\zeta_{1,2}(h\nu,x)=\zeta(h\nu,x)$ for the corresponding regions of the diode. The quantities ϵ_f and ϵ_b appearing in Eq. (2) are then given by

$$\epsilon_f=\int_0^\infty e^{-\mu_s x}[1-\zeta_1(x)]\mu_s dx \tag{A2}$$

and

$$\epsilon_b=\int_0^d e^{-\mu_s x}[1-\zeta_2(x)]\mu_s dx. \tag{A3}$$

μ_s is the linear absorption coefficient of silicon. Equations (A2) and (A3) transform the separate spatial regions, where ζ_1 and ζ_2 deviate from unity, into separate ranges of photon energy, where ϵ_f and ϵ_b deviate from zero. This avoids any correlation between the parameters l_{th} and r_i for ϵ_f on the one side and d, d_d and ϵ_{end} for ϵ_b on the other.

The model for $\zeta_1(h\nu,x)$ presented here is based on a model which had originally been developed for energy-dispersive Si(Li) detectors.[26] These detectors consist of a fully depleted layer of Li-compensated silicon 3 to 5 mm thick, with a gold-silicon Schottky contact at the radiation entrance. The idea of this so-called hot electron escape model is as follows: The final state of the impact ionization process, when all electrons and holes are slowed down to kinetic energies below the band gap, is still far from thermal equilibrium, and the further energy loss is due to phonon scattering with a mean free path of 7.6 nm for the 64 meV optical phonons.[36] The mean free path increases drastically when the kinetic energy of the electrons falls below the threshold for optical phonon scattering at 64 meV. During thermalization, the electrons diffuse over the thermalization range l_{th}, which is a property of silicon. The height of the Schottky barrier defines the reflection probability r_i of the nonthermal electrons at the gold-silicon interface. The pulse height distribution of the Si(Li) detectors could be described by integrating for each position x the distribution $\rho_e(h\nu,x,x'')$ within the silicon and adding the part outside times r_i. This implicitly includes the assumption that $c(x'')$ for thermal electrons is unity in the case of the Schottky barrier.

For a p-n junction detector with an oxide passivation, $c(x'')$ cannot be assumed to be unity,[48] on the other hand, the electrons cannot escape into the oxide during the thermalization, as the ionization threshold of about 2 eV is lower than the energy difference from the silicon conduction band minimum and the oxide conduction band minimum of 3.1 eV.[49] r_i must therefore by unity. In Ref. 48, $c(x'')$ was independently determined for the p-n junction detectors investigated. The thermalization length was thus the only free parameter which could be varied to fit the measured lineshapes. The values of $l_{th}=120$ nm obtained at 300 K and 170 nm at 140 K agree well with the 210 nm for the Si(Li) detector of Ref. 26 at 90 K. The concept of the representation of $\zeta_1(h\nu,x)$ by the convolution of $\rho_e(h\nu,x,x'')$ and $c(x'')$ has thus been proved for silicon p-n devices.

For photodiodes, the surface recombination can be adequately described using two parameter models for $c(x)$.[50] Possible expressions are: $c(x)=\epsilon_0+(1-\epsilon_0)\ x/x_0$ for $x<x_0$ (Ref. 51) or $c(x)=\epsilon_0+(1-\epsilon_0)(1-\exp(-x/x_0))$.[48] A simpler but less accurate model with only one parameter is that of a dead layer, $c(x)=0$ for $x<x_0$.[20]

Downloaded 19 Jun 2003 to 192.135.10.241. Redistribution subject to AIP license or copyright, see http://ojps.aip.org/japo/japcr.jsp

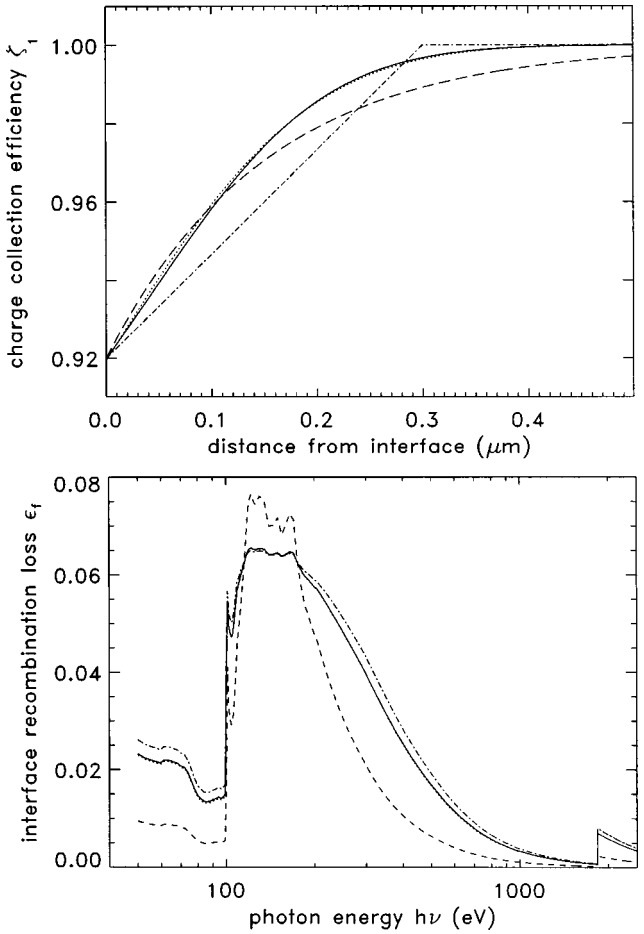

FIG. 12. Upper part: Models for $\zeta_l(x)$. Solid line: convolution of an exponential approximation for $c(x)$ with $x_0=45$ nm and $\epsilon_0=0.873$ with $\rho_e(x)$ defined by $l_{\text{th}}=120$ nm. Other functions are shown for comparison. The dotted line, nearly coincident with the solid line, represents the approximation by the hot electron escape model with $l_{\text{th}}=170$ nm and $r_i=84\%$. The long dashed line gives the exponential form with $x_0=150$ nm, and finally the dash-doted line the linear form with $x_0=300$ nm, ($\epsilon_0=0.92$ in both cases). Lower part: ϵ_f is shown as a function of the attenuation coefficient, calculated by Eq. (A2), using the models for ζ_l shown in the upper part. The styles of the (nearly coincident) lines are the same as in the upper part. The short dashed line shows the dead layer model for comparison.

As an example, $\zeta_1(x)$ was calculated using $\sigma=120$ nm for $\rho_e(x,x'')$ and the exponential approximation from Ref. 48 with $\epsilon_0=0.92$ and $x_0=45$ nm for $c(x'')$, solid line in Fig. 12. The values of ϵ_0 and x_0 are chosen to yield a good approximation of the spectral dependence of ϵ_f, obtained for the diodes used here. As convolution is not convenient for a fitting procedure, we tried to approximate $\zeta_1(x)$. The results are shown in the upper part of Fig. 12. We used the same value $\epsilon_0=0.92$ for all models. The hot electron escape model with $l_{\text{th}}=170$ nm and $r_i=84\%$, yields the best approximation, points in Fig. 12. Approximations using the linear and exponential representations as given above for $c(x)$ are shown for comparison. For s_r, however, ϵ_f is needed rather than $\zeta_1(x)$. It is shown as a function of photon energy in the lower part of Fig. 12. Please note that there are only minor differences between the models for $\zeta_1(x)$ shown in the upper part of Fig. 12. Only the dead layer model, which is shown for comparison in the lower part, deviates significantly. We therefore conclude that the error caused by the approximation of ϵ_f with the hot electron escape model is negligible.

The calculation of the backside transmission losses of the diodes, ϵ_b, in the same way as in Ref. 20 did not yield satisfying results. A main condition used in the derivation of the relation for solar cells, Ref. 36, is a homogeneous doping of the backside region. That does obviously not hold for the diodes investigated here, with an epitaxial layer on top of a high doped substrate. The basic result is, however, that the charge collection efficiency in the backside region drops continuously from unity to zero with the minority carrier diffusion length as the characteristic length. As a first approximation we used therefore a model with the charge collection efficiency linearly decreasing within the epitaxial layer, where the minority carrier diffusion length is rather long and abruptly decreasing to zero at the interface to the highly doped bulk, where the minority carrier diffusion length is very short. We get thus three parameters, the depletion depth d_d, defined as the depth till which the collection efficiency is unity, the thickness of the epitaxial layer, here d, and the collection efficiency at the interface to the bulk material, ϵ_{end}. This model yields a much better approximation than the original model with a constant diffusion length:

$$\epsilon_b = e^{(-\mu_s d)}\left[1+\frac{1-\epsilon_{\text{end}}}{\mu_s d^*}\left(e^{(\mu_s d^*)}-\mu_s d^*-1\right)\right]. \qquad \text{(A4)}$$

$d^*=d-d_d$ is used for a shorter notation. Typical values of ϵ_b for the diodes used here are: 0.05% at 0.8 keV, 0.35% at 1 keV, 1.5% at 1.3 keV, 2.9% at 1.5 keV, and 6.5% at 1.83 keV. ϵ_b is thus of no significance in the photon energy region below 500 eV, where possible changes of W were predicted. We put therefore no further effort on the refinement of this model.

In contrast to the manufacturer's statement, that the complete epitaxial layer of 35 μm should be depleted, we obtained a rather low result for $d_d=2$ μm, the value $\epsilon_{\text{end}}=85\%$, however, is rather high and $d=47$ μm is even slightly higher than the nominal thickness of the epitaxial layer, so that we believe that our fit results are in a reasonable agreement with the stated parameters of the photodiodes.

C. Electron and photon escape

The escape of primary electrons before they are slowed down leads to the loss not only of a single charge but also of the energy for further ionizations. In energy-dispersive detectors, events with an electron escape result in a charge pulse somewhere in-between zero and the maximum charge. This causes the so-called shelf in the pulse height spectra. The model of Ref. 26, which describes the shelf by the escape of energetic electrons from the detector volume as well as the detection of electrons from the detector front contact, is used here for silicon n-on-p diodes.

The probabilities P_{Aug} and P_{pho} that an (Auger or photo-) electron with an effective range R is generated at a distance $<R$ from the interface in a layer of total thickness d_l and passes the interface is calculated using an isotropic

Downloaded 19 Jun 2003 to 192.135.10.241. Redistribution subject to AIP license or copyright, see http://ojps.aip.org/japo/japcr.jsp

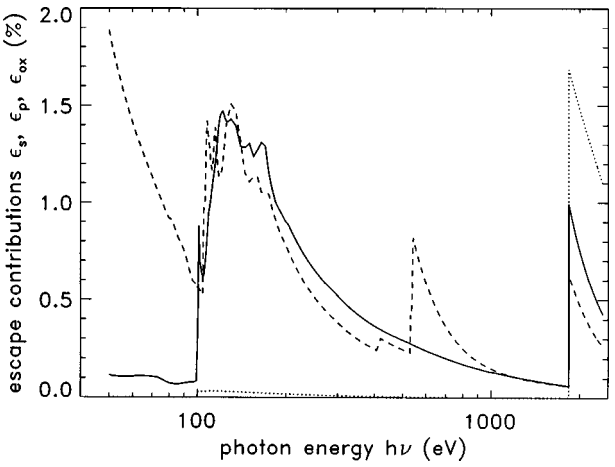

FIG. 13. Contributions of escape losses to the relative responsivity: electron escape loss ϵ_s (solid line), electron import from the surface layers ϵ_{ox} (dashed line) and photon escape loss ϵ_p (dotted line). Note that the signs of ϵ_s and ϵ_{ox} in Eq. (2) are opposite so that these contributions cancel each other for nearly all photon energies, except below 100 eV.

distribution of the initial direction for Auger electrons and a $\sin^2\Theta$ characteristic of the photoelectron emission:

$$P_{\mathrm{Aug}}=\begin{cases}\mu_s R/4 & R<d_l\\ \mu_s d_l/2\ (1-d_l/2R) & R>d_l\end{cases},$$
$$P_{\mathrm{pho}}=\begin{cases}3\mu_s R/16 & R<d_l\\ \mu_s d_l/2\ (1-3d_l/4R+d_l^3/8R^3) & R>d_l\end{cases}. \tag{A5}$$

The electron ranges $R(h\nu)$ were calculated using the approximation by Fitting[52] with a constant of 5 nm for the oxide and 3 nm for silicon added to take the nonvanishing mean free path of the electrons at low kinetic energies into account. The values are chosen in accordance with electron mean free path data[53] taking into account that the electrons from the silicon have to pass a potential barrier, due to the wider band gap of the oxide. ϵ_s and ϵ_{ox} are obtained as

$$\epsilon_x=\sum_i \frac{1/2\ E_i}{E_{h\nu}}\,P_{\mathrm{pho,Aug}}(x), \tag{A6}$$

where E_i are the initial electron energies, assuming that the average energy of the escaping electrons is just half their initial energy. This is justified by the flat spectral shape of the shelf in the pulse-height spectra of energy-dispersive detectors, which indicates equal probability for all values of the energy loss. The summation is over the most probable Auger and photoelectron energies, see Table III.

The escape contribution of fluorescence photons, ϵ_p, is calculated using the formula from Ref. 54 for the photon escape probability:

$$\epsilon_p=0.5\omega_k\,\frac{r_j-1}{r_j}\left[1-\frac{\mu_s}{\mu_k}\ln\left(1+\frac{\mu_k}{\mu_s}\right)\right]\frac{E_k}{h\nu}. \tag{A7}$$

E_K is the mean $K_{\alpha,\beta}$ photon energy, μ_k the attenuation coefficient for the fluorescence radiation, $\omega_K=0.052$ (Ref. 55) the fluorescence yield and $r_j=11$ (Ref. 38) the edge jump ratio. A similar expression with the much lower fluorescence yield of the L shell must be used below the K-shell energy but yields only a negligible contribution, see Fig. 13.

[1] ''International Lighting Vocabulary,'' CIE publication No. 17.4 (1987).
[2] ICRU Report 31, ISBN 0-913394-25-4 (1979).
[3] R. D. Ryan, IEEE Trans. Nucl. Sci. **NS-20**, 473 (1973).
[4] R. H. Pehl, F. S. Goulding, D. A. Landis, and M. Lanzlinger, Nucl. Instrum. Methods **59**, 45 (1968).
[5] J. Geist and C. S. Wang, Phys. Rev. B **27**, 4841 (1983).
[6] R. C. Alig, S. Bloom, and C. W. Struck, Phys. Rev. B **22**, 5565 (1980).
[7] R. C. Alig, Phys. Rev. B **27**, 968 (1983).
[8] J. H. Werner, S. Kolodinski, and H. J. Queisser, Phys. Rev. Lett. **72**, 3851 (1994).
[9] N. M. Durant, N. P. Fox, Metrologia **30**, 345 (1993).
[10] F. J. Wilkinson, A. J. D. Farmer, and J. Geist, J. Appl. Phys. **54**, 1172 (1983).
[11] S. Kolodinski, J. H. Werner, T. Wittchen, and H. J. Qeisser, Appl. Phys. Lett. **63**, 2405 (1993).
[12] J. Geist, J. L. Gardner, and F. J. Wilkinson, Phys. Rev. B **42**, 1262 (1990).
[13] J. Geist, Nucl. Instrum. Methods Phys. Res. A **378**, 343 (1996).
[14] G. W. Fraser, A. F. Abbey, A. Holland, K. McCarthy, A. Owens, and A. Wells, Nucl. Instrum. Methods Phys. Res. A **350**, 368 (1994).
[15] C. Butz Jörgensen, C. Oelsen, H. W. Schnopper, T. Lederer, F. Scholze, and G. Ulm, Nucl. Instrum. Methods Phys. Res. A **367**, 83 (1995).
[16] P. Lechner and L. Strüder, Nucl. Instrum. Methods Phys. Res. A **354**, 464 (1995); P. Lechner, R. Hartmann, H. Soltau, and L. Strüder, *ibid.* **377**, 206 (1996).
[17] R. P. Kraft, D. N. Burrows, G. P. Garmire, J. A. Nousek, J. R. Janesick, and P. N. Vu, Nucl. Instrum. Methods Phys. Res. A **361**, 372 (1995).
[18] E. M. Gullikson, R. Korde, L. R. Canfield, and R. E. Vest, J. Electron Spectrosc. Relat. Phenom. **80**, 313 (1996).
[19] H. Rabus, V. Persch, and G. Ulm, Appl. Opt. **36**, 5421 (1997).
[20] M. Krumrey and E. Tegeler, Rev. Sci. Instrum. **63**, 797 (1992).
[21] Value reevaluated from Ref. 20 using the new model of s_r to calculate the correction factor.
[22] D. Arnold and G. Ulm, Rev. Sci. Instrum. **63**, 1539 (1992).
[23] F. Scholze, H. Rabus, and G. Ulm, Appl. Phys. Lett. **69**, 2974 (1996).
[24] A. Owens, G. W. Fraser, A. Keay, A. Wells, K. J. McCarthy, S. F. Hill, E. A. Hughes, A. D. Smith, V. Suller, and M. Surman, X-Ray Spectrom. **25**, 33 (1996).
[25] A. Owens, G. W. Fraser, A. F. Abbey, A. Holland, K. McCarthy, A. Keay, and A. Wells, Nucl. Instrum. Methods Phys. Res. A **382**, 503 (1996).
[26] F. Scholze and G. Ulm, Nucl. Instrum. Methods A **339**, 49 (1994).
[27] K. Torii, H. Tsunemi, E. Miyata, and K. Hayashida, Nucl. Instrum. Methods Phys. Res. A **361**, 364 (1995).
[28] J. E. Martin, N. P. Fox, and P. G. Key, Metrologia **21**, 147 (1985).
[29] F. Lei and J. Fischer, Metrologia **30**, 297 (1993).
[30] N. P. Fox, Metrologia **32**, 535 (1995/96).
[31] A. Lau-Främbs, U. Kroth, H. Rabus, E. Tegeler, and G. Ulm, Rev. Sci. Instrum. **66**, 2324 (1995); A. Lau-Främbs, U. Kroth, H. Rabus, E. Tegeler, G. Ulm, and B. Wende, Metrologia **32**, 571 (1995/96).
[32] F. Scholze, M. Krumrey, P. Müller, and D. Fuchs, Rev. Sci. Instrum. **65**, 3229 (1994).
[33] H. Rabus, F. Scholze, R. Thornagel, and G. Ulm, Nucl. Instrum. Methods Phys. Res. A **377**, 209 (1996).
[34] AXUV100G from Intern. Rad. Detect.
[35] R. Korde, J. S. Cable, and L. R. Canfield, IEEE Trans. Nucl. Sci. **40**, 1655 (1993).
[36] S. M. Sze, *Physics of Semiconductor Devices* (Wiley, New York, 1981).
[37] F. Scholze, H. Rabus, and G. Ulm, Proc. SPIE **2808**, 534 (1996).
[38] B. L. Henke, E. M. Gullikson, and J. C. Davis, At. Data Nucl. Data Tables **54**, 181 (1993).
[39] A. Owens, K. J. McCarthy, and A. Wells, Proc. SPIE **2279**, 493 (1994).
[40] C. Chang, C. Hu, and R. W. Brodersen, J. Appl. Phys. **57**, 302 (1985).
[41] N. Sano, T. Aoki, M. Tomiszawa, and A. Yoshii, Phys. Rev. B **41**, 12122 (1990).
[42] N. Sano and A. Yoshii, Phys. Rev. B **45**, 4171 (1992).
[43] J. M. F. dos Santos, R. E. Morgado, L. M. N. Tavora, and C. A. N. Conde, Nucl. Instrum. Methods Phys. Res. A **350**, 216 (1994).
[44] L. C. Emerson, R. D. Birkhoff, V. E. Anderson, and R. H. Ritchie, Phys. Rev. B **7**, 1798 (1973).

Downloaded 19 Jun 2003 to 192.135.10.241. Redistribution subject to AIP license or copyright, see http://ojps.aip.org/japo/japcr.jsp

[45] C. Tarrio and S. E. Schnatterly, J. Opt. Soc. Am. B **10**, 952 (1993).
[46] E. D. Palik, *Handbook of Optical Constants of Solids* (Academic, Orlando, 1985).
[47] P. F. Morrissey, S. R. McCandliss, and P. D. Feldman, Appl. Opt. **34**, 4640 (1995).
[48] R. Hartmann, P. Lechner, L. Strüder, F. Scholze, and G. Ulm, Metrologia **32**, 491 (1995/1996).
[49] D. J. DiMaria and M. V. Fischetti, J. Appl. Phys. **64**, 4683 (1988).
[50] J. Geist, J. Appl. Phys. **51**, 3993 (1990).
[51] R. A. Stern, L. Shing, and M. M. Blouke, Appl. Opt. **33**, 2521 (1994).
[52] H.-J. Fitting, Phys. Status Solidi A **26**, 525 (1974).
[53] G. A. Somorjai, *Chemistry in two Dimensions: Surfaces* (Cornell University Press, Ithaka, 1981), p. 41.
[54] S. B. J. Reed and N. G. Ware, J. Phys. E **5**, 582 (1972).
[55] F. Schalze, *Quantenausbeute von Silicium für Photonen in Energiebereich von 50 eV bis 1500 eV* (Oberhofer, Berlin, 1997), p. 34.

Downloaded 19 Jun 2003 to 192.135.10.241. Redistribution subject to AIP license or copyright, see http://ojps.aip.org/japo/japcr.jsp